Journal of Power Sources 263 (2014) 75–84

Contents lists available at ScienceDirect

Journal of Power Sources

journal homepage: www.elsevier.com/locate/jpowsour

Cycle life analysis of series connected lithium-ion batteries with temperature difference

Kuan-Cheng Chiu [a], Chi-Hao Lin [b,c], Sheng-Fa Yeh [b], Yu-Han Lin [b], Chih-Sheng Huang [a], Kuo-Ching Chen [a,*]

[a] Institute of Applied Mechanics, National Taiwan University, 1, Sec. 4, Roosevelt Rd., Taipei 10617, Taiwan
[b] Material and Chemical Research Laboratories, Industrial Technology Research Institute, 195, Sec. 4, Chung Hsing Rd., Chutung, Hsinchu 31040, Taiwan
[c] National Center for Research on Earthquake Engineering, National Applied Research Laboratories, 200, Sec. 3, Hsin Hai Rd., Taipei 106, Taiwan

HIGHLIGHTS

- A cycle life model is proposed to simulate the capacity fade of LIBs.
- We simulate the discharge curve of series connected LIBs.
- Increased temperature difference among cells decreases the pack capacity.
- The adverse effect of temperature is experimentally verified.

ARTICLE INFO

Article history:
Received 28 November 2013
Received in revised form
16 February 2014
Accepted 7 April 2014
Available online 18 April 2014

Keywords:
Lithium-ion battery
Series connection
Cycle life
Temperature difference
Battery pack capacity fade

ABSTRACT

Within a battery pack of electric vehicles, a constant and homogeneous temperature distribution is an ideal case. However, what is in fact frequently observed is an unbalanced cycle life performance between series/parallel connected cells. While previous studies have proposed models that simulate the capacity fade of a single lithium-ion battery (LIB) in cycle life tests, most of them do not consider the accompanying effects when batteries are connected, and these models could only investigate cycling under a constant cell temperature. To analyze the temperature difference effect on a battery pack, we develop a cycle life model that allows for temperature variation of LIBs during cycling, and we apply the model to the simulation of series connected LIBs based on the porous electrode theory. We assign different hypothetical temperatures to each of the cells in series. Such a design generates a state of performance imbalance. Our result shows that the capacity degradation of the battery pack increases with the increase of temperature difference and of the average temperature. We then conduct an experiment to verify this adverse effect. The experimental data agree well with the simulation result.

1. Introduction

With an innate advantage of no memory effect and high power density, lithium-ion battery (LIB) is currently an ideal power source for electric powered vehicles [1–4]. However, one of the major concerns that limits the application and market of LIB in electric transportations is the life span of the cells. This cells' life span, which is often identified as the cycle life performance in the study of LIB, is highly determined by the cells' working temperature condition. Therefore, battery thermal management has been an important topic in the field of LIB application.

In industrial applications, a high voltage and power is usually required; hence, we need a battery pack that is composed of several batteries connected in series and parallel. Due to the cell layout inside the pack, the ideal scenario of no temperature difference is difficult to achieve. That is, it is challenging to keep uniform temperature between individual cells. Although it is well known that temperature difference will affect the capacity of battery pack [5,6], the degree of this influence yet requires further qualitative and quantitative analysis. Such analyses can be performed with the aid of battery pack simulation, which includes the modeling of LIB capacity fade and battery series/parallel connection.

* Corresponding author. Tel.: +886 2 3366 5676; fax: +886 2 2363 9290.
E-mail addresses: kcc@spring.iam.ntu.edu.tw, kuochingchen@ntu.edu.tw (K.-C. Chen).

http://dx.doi.org/10.1016/j.jpowsour.2014.04.034
0378-7753/

Since cycle life degradation is mainly contributed by the side reactions of lithium-ion and electrolyte, the induced irreversible current, which may co-exist with the reversible current, can be considered as the cause of the capacity fade [7–10]. Put differently, the irreversible reaction triggers a continuous loss of active material during every cycle. Therefore, numerical modeling of this process can also be achieved by decreasing a specific amount of the initial lithium-ion concentration before each discharge [11]. Another option to simulate LIB cycle life is to use the single particle model [12]. This alternative approach is to concentrate only on modeling the SEI growing behavior at the porous negative electrode's surface and calculate the equivalent battery capacity loss. Other cycle life simulations also take temperature into account [13,14], as experiments have shown that a higher cell temperature results in a poorer cycling ability [13].

Although numerous studies have presented models that can simulate the capacity fade of an LIB [7–15], a majority of them are limited to the assumption of constant battery temperature, which is difficult to maintain for a large C-rate discharge. Moreover, this isothermal assumption deviates far from the situation of an LIB in practice, where various factors can cause the battery temperature to fluctuate frequently and severely. For this reason, it is necessary to develop a new model with the ability to consider the temperature variation of an LIB. On the other hand, there may be dozens of cells connected in series/parallel within a particular battery pack; however, simulations of series/parallel connected LIBs were seldom performed, especially by an electrochemical approach. Consequently, a simulation of series/parallel connected battery that takes temperature as an important parameter would be critical in the study of LIB pack cycle life performance.

It has been known that both parallel and series connection have additional, probably negative, effects on the battery pack's performance. However, they affect the pack performance in distinct ways. Different from a series-connected pack where cells share the same value of electric current, the current in a single battery of a parallel-connected pack could differ from each other due to mismatching resistance that might be induced by unbalanced temperature between cells. The topic of mismatching internal resistance of cells has recently been studied with experiments [16], and it has been shown that matching resistance of cells is crucial in the cycle-life of a parallel connected pack. Accordingly, one of the key issues to be explored in modeling a parallel-connected pack is to find a robust or efficient way that could renew or adjust the distribution of total electric current in accordance with the timely change in cell's impedance. The aforementioned issues of a parallel-connected pack deserve an independent study and are therefore beyond our scope. In this paper, for simplicity of analysis and for the sole purpose of evaluating the effect of temperature difference on the cycle life performance of a battery pack, we focus our attention on a series connection.

The study models a battery pack that consists of ten series connected cells. The batteries are 26650 lithium iron phosphate (LFP) 2.3 Ah LIBs, a type of cell that has received great interest in the recent years in both academic and industrial fields [13,14,17–25]. Based on the porous electrode theory, we develop a numerical model which allows variation of temperature. First, we find the discharge curve for a single LIB. The capacity fade is described by a newly proposed Arrhenius type equation, which accounts for the irreversible decrease in the lithium-ion concentration of negative electrode in the discharge process. Afterward, to investigate the temperature difference effect on the pack's cycling performance, this single LIB model is applied to a series-connected pack, where a temperature distribution of the assembly is specified.

Conducting a full-scale experiment of cycling multiple connected batteries of different temperature will take a considerable amount of time. However, in order to verify the result of our simulation, we conduct a smaller-scale experiment, where two cells are connected in series, to examine whether temperature difference has an effect on the performance of the batteries. The model developed here can be used to estimate the performance of a battery pack with specific thermal management by simulation. Accordingly, this work could provide a relatively time- and money-saving solution for the development of battery packs.

2. Galvanostatic discharge curves of an LIB

Based on a series of works by Newman's group [26–30], the porous electrode theory is currently widely used in simulating the electrochemical process of LIBs. The model simplifies the jelly-roll of the cell to a one-dimensional geometry that is composed of five segments which correspond to the thickness of two current collectors, of two electrodes, and of a separator. Fig. 1 is an example of the one-dimensional structure, where the leftmost boundary of the left current collector is set as the origin of the x-axis in our study.

The solid phase materials of the porous electrodes are treated as a series of lithium containing spherical particles aligned along the x-axis. In the solid phase the mass transfer of lithium can be described by the spherical Fick's laws of diffusion which occurs within the particle at position x:

$$\frac{\partial C_{s,i}(x,r,t)}{\partial t} = D_{s,i}\left[\frac{\partial^2 C_{s,i}(x,r,t)}{\partial r^2} + \frac{2}{r}\frac{\partial C_{s,i}(x,r,t)}{\partial r}\right], i = n,p, \quad (1)$$

where $C_{s,i}$ is the concentration of lithium in the i electrode, $D_{s,i}$ is the solid phase lithium diffusivity, r is the radial coordinate of the electrode's particle, and the subscripts n and p denote the negative and positive electrode, respectively.

At the surface of the electrodes, the net pore wall flux of lithium-ion can be evaluated by the Butler–Volmer equation

$$j_i = k_i(c_i)^{0.5}\left(C_{s,i,\max} - C_{s,i,\text{surf}}\right)^{0.5}\left(C_{s,i,\text{surf}}\right)^{0.5} \times \left[\exp\left(\frac{F\eta_{s,i}}{2RT}\right) - \exp\left(\frac{-F\eta_{s,i}}{2RT}\right)\right], \quad i = n,p, \quad (2)$$

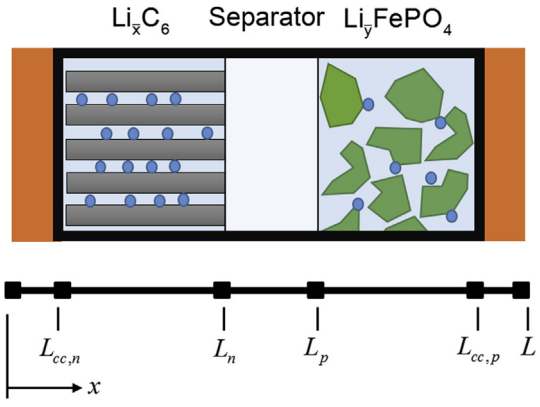

Fig. 1. The one-dimensional geometry of porous electrode theory.

where the surface overpotential at the electrodes $\eta_{s,i}$ is expressed by

$$\eta_{s,i}(x,t) = \phi_{s,i}(x,t) - \phi_{l,i}(x,t) - U_i^c(x,t) - Fj_i(x,t)R_{f,i}, \quad i = n,p. \tag{3}$$

Here, k_i, c_i, F, R, $\varphi_{s,i}$, $\varphi_{l,i}$, and U_i^c are the reaction rate constant, concentration of salt in electrolyte, Faraday's constant, gas constant, electrical potential of solid phase, electrical potential of electrolyte phase, and open-circuit potential (OCP), respectively. Considering the mechanism of SEI film formation, the film resistance R_f is assumed to exist only at the porous negative electrode's side [31]. The last term of Equation (3) is thus neglected for the porous positive electrode.

According to the conservation of charge and Ohm's law, the relation between the pore wall flux of lithium-ion j_i and electrode potential of solid phase is written as

$$\sigma_i^{\text{eff}}\frac{\partial^2\phi_{s,i}(x,t)}{\partial x^2} = Fa_ij_i, \quad i = n,p, \tag{4}$$

where σ_i^{eff} is the effective conductivity and a_i is the specific interfacial area. They are determined by $\sigma_i^{\text{eff}} = \sigma_i(1-\varepsilon_{s,i}-\varepsilon_{f,i})$ and $a_i = 3(1-\varepsilon_{s,i}-\varepsilon_{f,i})/R_{s,i}$, where σ_i, $\varepsilon_{s,i}$, $\varepsilon_{f,i}$, and $R_{s,i}$ stand for the solid-phase electric conductivity, porous electrode volume fraction, filler volume fraction, and radius of electrode particle, respectively.

The electrolyte contains both cations and anions. This means that the charge transfer in the electrolyte phase is more complicated than in the solid phase. A modified Ohm's law can be utilized to account for the concentration gradient effect of ions on the electrolyte phase potential:

$$-\kappa_i^{\text{eff}}\frac{\partial\phi_{l,i}(x,t)}{\partial x} - \sigma_i^{\text{eff}}\frac{\partial\phi_{s,i}(x,t)}{\partial x} + \frac{2\kappa_i^{\text{eff}}RT}{F}\left(1-t^+\right)\frac{\partial\ln c_i(x,t)}{\partial x} = I_{\text{app}}, \quad i = n,p,e, \tag{5}$$

where κ_i^{eff} is the effective electrolyte phase ionic conductivity, t^+ is the transference number, I_{app} is the applied current density, and $i = e$ signifies the separator region. Note that because no electron flows through the separator, the second term of Equation (5) does not apply in the case of $i = e$.

The concentration of lithium-ions in the electrolyte phase is obtained with the help of the concentrated solution theory [27], which explains the physics that governs diffusion, migration, and the flux of lithium-ion at the porous electrode surface due to redox reactions. From this theory we have

$$\varepsilon_{l,i}\frac{\partial c_i(x,t)}{\partial t} = D_{e,i}^{\text{eff}}\frac{\partial^2 c_i(x,t)}{\partial x^2} - \frac{I_{\text{app}}}{F}\frac{\partial t^+}{\partial x} + \frac{a_i}{\upsilon_+}\left(1-t^+\right)j_i(x,t), \quad i = n,p,e, \tag{6}$$

where υ_+ is the stoichiometric coefficient of lithium ion and $D_{e,i}^{\text{eff}}$ is the effective diffusion coefficient, which is modified by $D_{e,i}^{\text{eff}} = D_{e,i}\varepsilon_{l,i}^{\gamma}$. The modification is based on the porous effect, and $\varepsilon_{l,i}$ and γ represent the electrolyte volume fraction and the Bruggman exponential, respectively. In addition, the electrodes' OCPs at 25 °C for the LIB we adopted are [22]

$$\begin{aligned} U_{0,p}^c =& 3.4323 - 0.8428\exp\left[-80.2493(1-\overline{y})^{1.3198}\right] \\ &- 3.2474\times10^{-6}\exp\left[20.2645(1-\overline{y})^{3.8003}\right] \\ &+ 3.2482\times10^{-6}\exp\left[20.2646(1-\overline{y})^{3.7995}\right], \end{aligned} \tag{7}$$

and

$$\begin{aligned} U_{0,n}^c =& 0.6379 + 0.5416\exp(-305.5309\overline{x}) \\ &+ 0.044\tanh\left(\frac{0.1958-\overline{x}}{0.1088}\right) - 0.1978\tanh\left(\frac{\overline{x}-1.0571}{0.0854}\right) \\ &- 0.6875\tanh\left(\frac{\overline{x}+0.0117}{0.0529}\right) - 0.0175\tanh\left(\frac{\overline{x}-0.5692}{0.0875}\right), \end{aligned} \tag{8}$$

where $\overline{y}$ and $\overline{x}$ denote the state of charge of the positive electrode and of the negative electrode, respectively.

The values of the required parameters for simulating the 26650 2.3 Ah LFP cell via the porous electrode theory are listed in Table 1. Some of the parameters, such as electrode thickness, lithium concentration, and specific capacity, can be determined by conducting simple calculations or measurements. However, due to the various manufacturing processes and treatments of battery material by manufacturers, several material parameters proposed in previous works [14,22], such as diffusivity, film resistance and conductivity, need to be adapted for the batteries used for this study. Moreover, parameters such as porosity, particle size and reaction rate, are the ones that are usually difficult to be measured or calculated, so they can only be considered as the equivalent values in modeling. These parameters would be estimated so as to obtain the simulated galvanostatic discharge curves which best fit the experimental data. Furthermore, harsh operating conditions, such as high C-rate discharge or lack of battery thermal management, may lead to a considerable increase in cell temperature, thus altering the temperature sensitive parameters of the battery severely. These parameters and their dependencies on temperature used in this study are shown in Table 2.

Given the required initial and boundary conditions, we are able to solve the time- and space-dependent variables of the porous electrode theory, which are $\varphi_{s,n}$, $\varphi_{s,p}$, $\varphi_{l,n}$, $\varphi_{l,p}$, $\varphi_{l,e}$, $C_{s,n}$, $C_{s,p}$, c_n, c_p, c_e, j_n, j_p, U_n^c, and U_p^c, by numerical iteration. Fig. 2 shows the comparison between the simulated discharge curves and the corresponding experimental data [22] for the 26650 2.3 Ah LFP cell in a 0.1 C–3 C galvanostatic discharge at 25 °C. The good agreement between the two results, especially in describing the cell's capacity, indicates that the porous electrode theory is valid to model the electrochemical process of a single LIB. Therefore, it will be utilized in the simulation of the capacity fade of a pack of LIBs, as we report in the following.

Table 1
Electrochemical parameters of the 26650 LFP 2.3 Ah cell.

Parameter	Negative electrode	Separator	Positive electrode
$D_{s,i,0}$ ($m^2\ s^{-1}$)	3.9×10^{-14} [a]	–	1.18×10^{-18} [a]
$R_{f,i}$ ($\Omega\ m^2$)	0.06[d]	–	–
σ_i ($S\ m^{-1}$)	100[a]	–	0.5[a]
$R_{s,i}$ (μm)	1.05[d]	–	0.0365[b]
$\varepsilon_{s,i}$	0.55[a]	–	0.43[a]
$\varepsilon_{l,i}$	0.33[a]	1	0.332[a]
$C_{s,i,\max}$ ($mol\ m^{-3}$)	31,370[a]	–	22,806[a]
$C^0_{s,i,\text{surf}}$ ($mol\ m^{-3}$)	25096[a]	–	684.18[a]
$k_{i,0}$ ($m^{2.5}\ mol^{-0.5}\ s^{-1}$)	3×10^{-12} [d]	–	1.4×10^{-12} [a]
L_i (μm)	34[a]	30[a]	70[a]
$D_{e,i,0}$ ($m^2\ s^{-1}$)	–	3.227×10^{-10} [a]	–
t^+		0.363	–
A_{cell} (m^2)		0.173[c]	

[a] Ref. [14].
[b] Ref. [22].
[c] Estimated.
[d] Fitted.

Table 2
The temperature dependent parameters of the 26650 LFP 2.3 Ah cell.

Parameter	Expression
$D_{s,n}$ [a]	$D_{s,n,0}\exp\left[\frac{35000}{R}\left(\frac{1}{298.15}-\frac{1}{T}\right)\right]$
$D_{s,p}$ [a]	$D_{s,p,0}\exp\left[\frac{35000}{R}\left(\frac{1}{298.15}-\frac{1}{T}\right)\right]$
k_n [a]	$k_{n,0}\exp\left[\frac{20000}{R}\left(\frac{1}{298.15}-\frac{1}{T}\right)\right]$
k_p [a]	$k_{p,0}\exp(-3\bar{y})\exp\left[\frac{35000}{R}\left(\frac{1}{298.15}-\frac{1}{T}\right)\right]$
$D_{e,i}$ [a]	$1\times10^{-4}\times10^{-4.43-\frac{54}{T-229-0.005c_i}-2.2\times10^{-4}c_i}$
κ_i^{eff} [b]	$1\times10^{-4}c_i\left(\begin{array}{l}-10.5+0.074T-6.96\times10^{-5}T^2+6.68\times10^{-4}c_i\\-1.78\times10^{-5}c_iT+2.8\times10^{-8}c_iT^2+4.94\times10^{-7}c_i^2\\-8.86\times10^{-10}c_i^2T\end{array}\right)^2$

[a] Ref. [14].
[b] Ref. [32].

3. LIB capacity fade

Although there may be several side reactions during the discharge/charge process in batteries, the capacity fade of LIBs is mainly caused by the irreversible reactions between lithium-ion and electrolyte in the electrochemical system [7,11–13,31,33]. Some examples of such reactions are presented as follows in the case of an EC/DMC electrolyte and 1 M of $LiPF_6$ [33]:

$$\begin{aligned}
&2EC + 2e^- + 2Li^+ \rightarrow (CH_2OCO_2Li)_2\downarrow + CH_2 = CH_2\\
&EC + 2e^- + 2Li^+ \rightarrow LiCH_2CH_2OCO_2Li\downarrow\\
&DMC + e^- + Li^+ \rightarrow \dot{C}H_3 + CH_3OCO_2Li\downarrow + CH_3OLi\downarrow + CH_3\dot{O}CO\\
&H_2O + e^- + Li^+ \rightarrow LiOH\downarrow + 1/2H_2\\
&LiOH + e^- + Li^+ \rightarrow Li_2O\downarrow + 1/2H_2\\
&H_2O + (CH_2OCO_2Li)_2 \rightarrow Li_2CO_3\downarrow + CO\\
&2CO_2 + 2e^- + 2Li^+ \rightarrow Li_2CO_3\downarrow + CO.
\end{aligned} \tag{9}$$

Considering the potentials of the two electrodes, it is more likely that these parasitic reactions take place at the negative side than at the positive one [31]. As a result, there would be a layer of deposit on the surface of the porous negative electrode. This layer is known as the SEI film, which induces the SEI resistance in the overpotential of the negative electrode reaction. When the battery is further cycled, cracks of the SEI film are formed due to continuous electrode expansion and contraction caused by the intercalation/deintercalation of lithium. These cracks provide a channel for the electrolyte to have direct contact with the electrode, thus forming new SEI film that fills the vacant and increases the thickness of the original layer [31]. The whole process is repeated during the charge and discharge cycles, and lithium-ion is constantly reduced to irreversible substances. Consequently, the concentration of active lithium-ion decreases, leading to the fade of LIB discharge capacity. A diagram of this development of SEI film is displayed in Fig. 3.

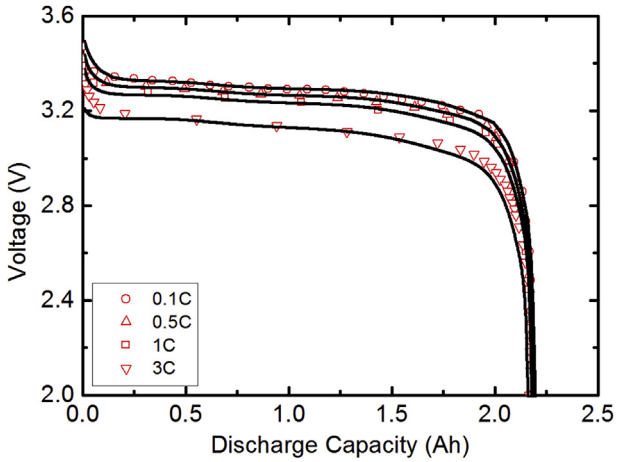

Fig. 2. The discharge curve of 26650 LFP 2.3 Ah LIB. The red markers are the experiment result [31], and the solid lines are from simulation with the assumption of constant cell temperature. (For interpretation of the references to color in this figure legend, the reader is referred to the web version of this article.)

3.1. Simulating capacity fade

In order to simulate the capacity fade of an LIB, an additional equation that describes the main irreversible process, which includes the concentration degradation of lithium-ions and the increase in thickness of SEI film, is required. In this study, we only consider the former effect while the latter is assumed to be minor, i.e., the growth of the SEI layer is neglected and the film resistance is kept constant. This is because the specific characteristic of an SEI resistance increase, which causes a downward shift of the voltage plateau [12], was not observed from the best fit of our preliminary simulation to the experimental result of the 26650 LFP 2.3 Ah battery cycling test. For the description of the former effect, we introduce a time-dependent parameter, $C_{\text{irr},N}(t)$, which represents the accumulated loss of lithium-ion concentration within the discharging process of the N-th cycle. The introduced parameter is aimed to evaluate the amount of active lithium-ion on the negative electrode at the beginning of each cycle. To this end, we propose that the lithium-ion concentrations in the negative electrode at the beginning of N-th and $(N+1)$-th cycles are satisfied by

$$C_{s,n,N+1}(x,r,0) = C_{s,n,N}(x,r,0) - C_{\text{irr},N}(t)\big|_{t=\tau_N}, \tag{10}$$

where t is the discharge time at each cycle and τ_N indicates the total discharge time when the battery reaches the discharge cut-off voltage of the N-th cycle. Note that the capacity of the cell is continuously fading, which implies that as N increases, τ_N decreases.

Since the cycle life performance of most LIBs strongly depends on the cells' temperatures [12,13], we assume that the time derivative of $C_{\text{irr},N}$, which represents the degradation rate, is expressed by a standard Arrhenius expression

$$\frac{dC_{\text{irr},N}(t)}{dt} = A_d \exp\left[\frac{-E_a}{RT(t)}\right]. \tag{11}$$

Here the two newly introduced parameters A_d and E_a represent the reference concentration degradation rate and the activation energy, respectively. They are set to be temperature independent as they are used in a standard Arrhenius expression, whereas the magnitude of C-rate is expected to have an influence on the value of A_d. We see immediately that the fact of a higher temperature resulting in a larger capacity fade [5,6] is reflected on the right-hand side of Equation (11), which illustrates that $dC_{\text{irr},N}/dt$ increases as temperature rises. It should be noted that because $C_{\text{irr},N}$ is the total concentration loss of active lithium-ion caused by the various irreversible side reactions shown in Equation (9), the combined characteristics of these reactions are equivalently described by the two parameters A_d and E_a.

From Equation (11), the parameter $C_{\text{irr},N}|_{t=\tau_N}$ is solved by integration over the time period τ_N:

$$C_{\text{irr},N}\big|_{t=\tau_N} = \int_0^{\tau_N} A_d \exp\left[\frac{-E_a}{RT(t)}\right] dt, \tag{12}$$

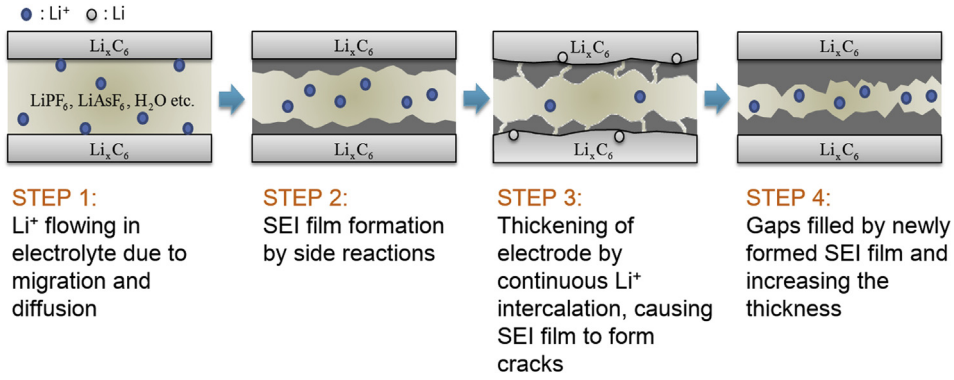

Fig. 3. The process of SEI thickening caused by side reactions of the LIB.

where use of the initial condition $C_{\mathrm{irr},N}(0) = 0$ is made. Although the parameters of the above equations do not explicitly include the discharging C-rate, the influence of different discharging current magnitudes is reflected on the temperature $T(t)$ and the total discharge time τ_N. This is due to the fact that a greater discharge rate would lead to a larger temperature rise and a shorter discharge time. In addition, the loss of active lithium-ion during the charging process is not considered in our modeling, which assumes that the lithium-ion degradation rate corresponds only to the conditions of discharge. Thus the value of $C_{\mathrm{irr},N}|_{t=\tau_N}$ would be regarded as the total loss of lithium-ion during charging and discharging in real situations.

3.2. Model verification

The two newly introduced parameters A_{d} and E_{a} need to be determined before $C_{\mathrm{irr},N}$ can be obtained. Technically, a larger A_{d} corresponds to a faster decay of the cell's capacity at the same temperature, and an increasing E_{a} indicates a higher level of difficulty for the irreversible reactions to proceed. To obtain A_{d} and E_{a}, we need two sets of experimental capacity fade data [13], i.e., two curves in the plot of capacity versus cycle number, of the 26650 LFP 2.3 Ah cell cycled under two different temperatures, which are 45 °C and 60 °C. The ratio of the slopes of the two curves is referred to as the ratio of the capacity fading rate, which is assumed to be the ratio of the two degradation rates, defined in Equation (11), for 45 °C and 60 °C. This assumption enables us to determine the parameter E_{a}. With the help of Equation (11), one can obtain the other parameter A_{d} by evaluating (i) the amount of Li-ion concentration that is decreased per cycle, ΔC_{irr}, (ii) the exponential term $\exp(-E_{\mathrm{a}}/RT)$ with $T = 318$ K or 333 K, and (iii) the discharge time τ_N for the cycled 0.5 C-rate, where τ_N for each cycle can be calculated as soon as the given discharge cut-off voltage is reached. For the battery we are modeling, we find that $A_{\mathrm{d}} = 142.35\ \mathrm{mol\ m^{-3}\ s^{-1}}$, and $E_{\mathrm{a}} = 3.39 \times 10^4\ \mathrm{J\ mol^{-1}}$.

The compared discharge curves of the cell cycled at 45 °C are shown in Fig. 4(a), where the solid lines represent our simulation result, and the red markers are from a previous experiment [13]. The cell is discharged at 0.5 C to a cut-off voltage 2.5 V, and its temperature is assumed to remain unchanged throughout the whole process. The capacity of the cell after 1707 charge/discharge cycles at this temperature has decayed by almost 21%. Since the cell is discharged at a very low C-rate in this cycle life test, the assumption of a constant battery temperature would be acceptable in this simulation.

In addition to cycling the battery at 45 °C, we simulate the capacity fade of the cell with a constant temperature of 60 °C, and the result, which also agrees well with the experiment [13], is shown in Fig. 4(b). Since the temperature is raised, the cell capacity has faded by almost 20% through only 754 cycles (Compare this result with the 21% fade after 1707 cycles at 45 °C).

3.3. Model advantages

Although there exist numerous approaches to model the capacity fade of an LIB [7,11–15,31], our method demonstrates several advantages described as follows.

First, our simulation is developed based on electrochemical governing equations in the porous electrode theory. By doing so, we

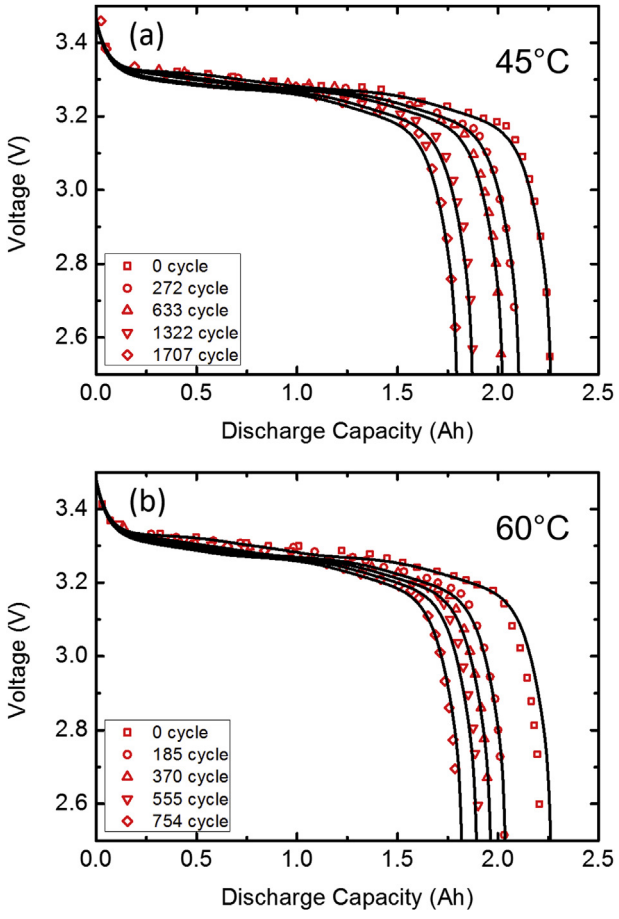

Fig. 4. Simulation (solid line) and experimental result (markers) of the 26650 LFP 2.3 Ah cell cycled (a) at 45 °C and (b) at 60 °C.

can not only calculate the capacity of an LIB during different cycles, but also trace out the corresponding discharge curves, which provide information about the variation of battery voltage with time.

Second, we describe the loss of Li-ion concentration within the discharging process by simply using Equation (12), where only two parameters A_d and E_a are involved and they can be determined by experimental capacity fade data. This advantage is not found in a relevant work [11], in which the loss of Li-ion concentration is associated with the proposed local parasite reaction current density j_{para}, which is assumed to follow a Tafel relation. Even if j_{para} can be utilized to calculate the increase in thickness of the SEI film and the decrease in Li-ion concentration at every cycle, the determination of j_{para} requires numerous equations and parameters and thus increases the difficulty and complexity of using such a model for simulation.

Third, we allow the battery's temperature to be a time dependent variable in the integrand of Equation (12) to calculate the total loss of active lithium-ion concentration. That is, our model can simulate the capacity fade of LIB with fluctuating temperature or at a high C-rate discharge where temperature change is apparent. This advantage is not available in another model [13,14], where a function of capacity fading rate Q_{loss} analogous to our Arrhenius expression in Equation (11) is proposed to deal with the total loss of Li-ion after specific cycles. The use of Q_{loss} makes it infeasible to consider the influence of temperature change during cycling. As a result, the assumption of constant cell temperature is required.

Fourth, apart from temperature, the cycle-by-cycle calculation enables us to explore other parameter alterations of the electrochemical system that may accompany cycling. For example, the contingent effects of electrode material dissolution and electrolyte decomposition, which have been reported to be associated with overcharge or overdischarge [34–41], could be reflected on the discharge curve. This can be simulated by adjusting certain material parameters at any cycle. Moreover, batteries cycled under manipulated operational conditions, which may include different cooling air flow, discharging C-rate, or discharging cut-off voltage, could also be simulated.

To sum up, our approach founds itself on the electrochemical theory. It has the strengths of considering temperature change, having fewer parameters to be determined, and allowing a larger degree of freedom in simulating the cycle life performance of an LIB.

4. Description of series connected LIBs

By using a porous electrode model for every single cell, the electrochemical process of series connected LIBs can be simulated. For M cells connected in series, we would need M sets of the model's equations described in the previous section to simulate the discharge curve of the pack. Given these equations, we then applied the continuity condition of voltage at all the connection nodes between adjacent series connected batteries, so that the k-th cell's negative current collector potential is the same as the $(k-1)$-th cell's positive current collector potential, i.e.,

$$\phi^k_{cc,n}|_{x=0} = \phi^{k-1}_{cc,p}|_{x=L}, \quad k = 2 \sim M. \tag{13}$$

The potential of the negative current collector in the first cell is set to zero, indicating ground connection:

$$\phi^1_{cc,n}|_{x=0} = 0. \tag{14}$$

The whole one-dimensional geometry for the model of M series connected LIBs is shown in Fig. 5.

5. Simulation of temperature difference effect on series connected batteries' cycle life performance

We now extend our scope to analyze the cycle life performance of LIBs connected in series with temperature difference. A battery pack of ten 26650 LFP 2.3 Ah LIBs connected in series is studied, and the temperature of each cell is assigned a different value to simulate the temperature difference effect. In order to make the analysis as simple as possible, a linear variation of temperature among different batteries in the pack is given. Fig. 6 consists of two groups of temperature distribution. The first group, which is in the lower part, includes three cases of temperature distribution: no temperature difference ($\Delta T = T_{10} - T_1 = 0$ °C), a 9 °C temperature difference ($\Delta T = 9$ °C), and an 18 °C temperature difference ($\Delta T = 18$ °C). They have the same average value of 34 °C. The second group includes another three cases with the same temperature differences, but with a higher average value, i.e., 60 °C. It should be noted that although the temperature difference in our design is larger than is likely to happen in normal operating battery packs, we believe that the quantitative and qualitative analyses of the extreme situations would help us to identify and understand the cycle life performance of an LIB pack due to temperature imbalance.

5.1. Simulation result

With the assigned temperature distribution for the individual cells, the pack is cycled 2000 times with a 0.5 C constant current discharge. Fig. 7(a) shows the discharge curves of the pack where all the cells are maintained at 34 °C ($T_{avg} = 34$ °C, $\Delta T = 0$ °C). Since there are ten LFP cells connected in series, the voltage of the pack before discharge is close to 35 V. However, the pack voltage will start to drop due to the passage of a current. The capacity of the pack is then captured when its output voltage reaches a given cut-off value, which is set as 30 V. When the pack is operated, the initial lithium-ion concentration at the negative electrode of each cell for each cycle decreases by a certain amount, calculated in Equation (12). Consequently, the capacity of the pack gradually deteriorates, and after repeating 2000 times of constant current discharge, the irreversible side reactions of the LIBs cause the capacity of the whole pack to reduce by 0.45 Ah, which is a 19% fade with respect to the nominal 2.3 Ah.

If there exists a temperature distribution ($\Delta T \neq 0$ °C), the reduced capacity is expected to increase due to an unbalanced performance among the cells. Fig. 7(b) demonstrates this increase

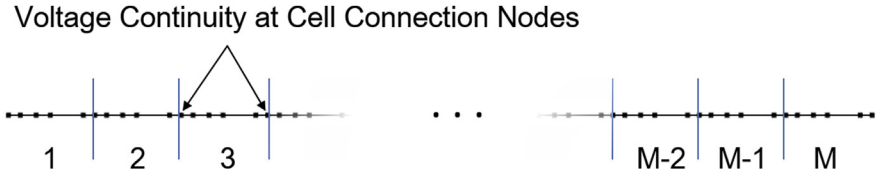

Fig. 5. The one-dimensional geometry for the M series connected porous electrode model.

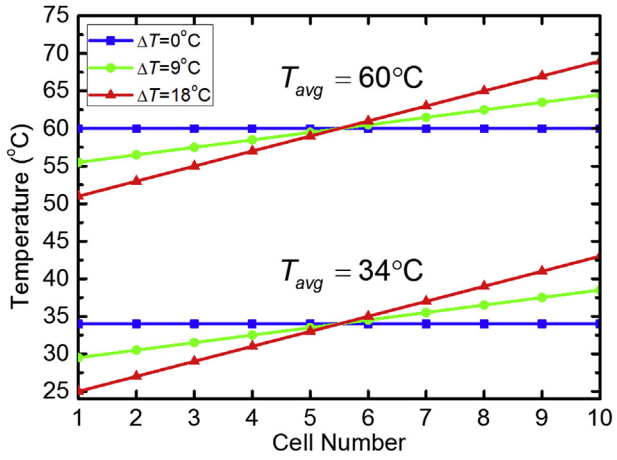

Fig. 6. Temperature distributions of the ten cells with an average value of 34 °C and with 60 °C.

in the case of $T_{avg} = 34$ °C and $\Delta T = 18$ °C. After 2000 cycles, the capacity of the pack has reduced by 22%, which is larger than the 19% fade in the case of no temperature difference.

The 3% difference in reduced capacity after 2000 cycles between $\Delta T = 0$ °C and $\Delta T = 18$ °C for the case of $T_{avg} = 34$ °C may not be sufficient to elucidate the influence of temperature difference. However, if the average temperature is raised and the same temperature distribution is applied to the battery pack, the influence would be more significant. Fig. 8(a) illustrates the case of isothermal battery pack ($\Delta T = 0$ °C) at $T_{avg} = 60$ °C, where a 38% capacity fade is obtained after 2000 cycles. By applying a temperature difference of $\Delta T = 9$ °C, it results in a 39% decay in capacity, and an astonishing 45% degradation for $\Delta T = 18$ °C is seen in Fig. 8(b). In addition to a larger capacity fade, a higher average temperature causes other undesired effects. By examining the discharge curves of $T_{avg} = 60$ °C in Fig. 8, we observe that there exists a large voltage gap, indicated by two blue arrows, between different cycles. This characteristic is not found on the discharge curves of $T_{avg} = 34$ °C in Fig. 7, where a high voltage plateau during cycling is observed. Furthermore, the higher average temperature $T_{avg} = 60$ °C leads to a steeper tangent in the discharge curve at lithium-ion depletion (the blue dash dotted line) with increasing temperature difference, that is, the voltage of battery pack drops more rapidly near the end of discharge. These are all negative effects of the cycle life performance of a battery pack caused by the temperature differences.

5.2. Discussion

The characteristics of a battery pack are determined by the individual cells that form the assembly. Therefore, to gain a

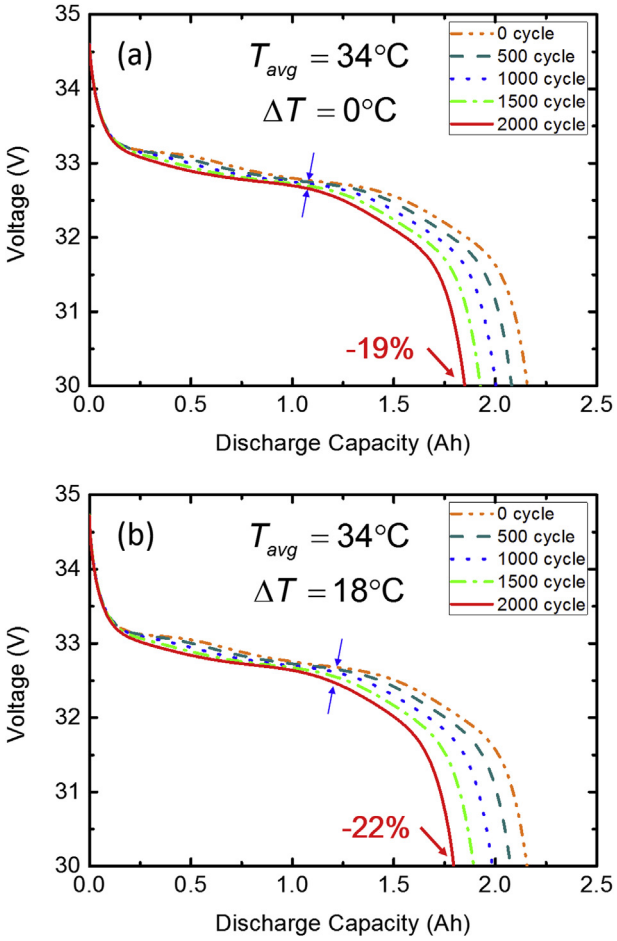

Fig. 7. Simulated capacity fade result of ten cells connected in series with $T_{avg} = 34$ °C when (a) $\Delta T = 0$ °C and (b) $\Delta T = 18$ °C.

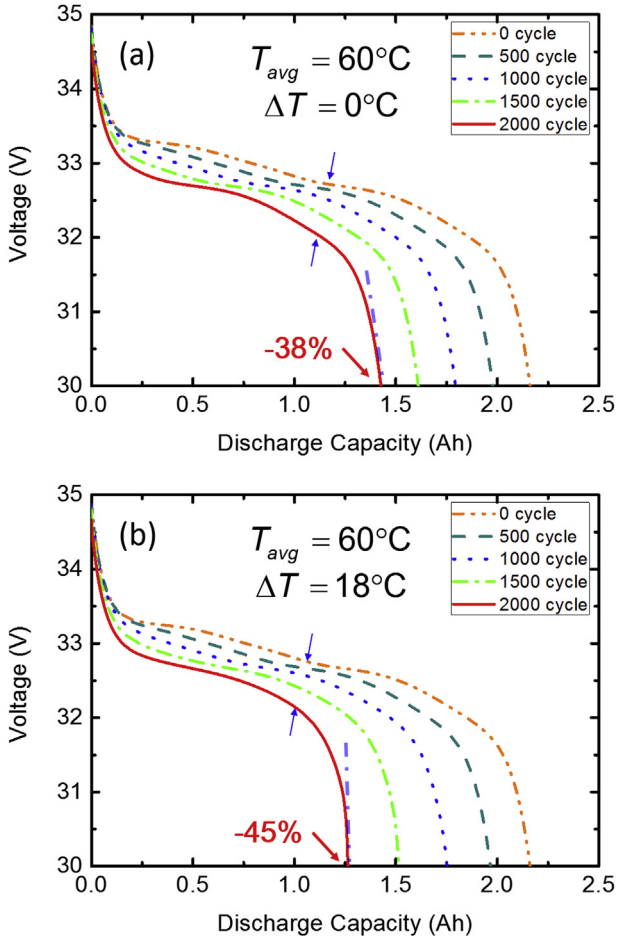

Fig. 8. Simulated capacity fade result of ten cells connected in series with $T_{avg} = 60$ °C when (a) $\Delta T = 0$ °C and (b) $\Delta T = 18$ °C.

deeper understanding of the temperature effect, we plot the discharge curves of the ten cells to distinguish the contribution of each to the overall pack performance. Shown in Fig. 9 is the 2000th cycle discharge curve of the case, which is a battery pack of $T_{avg} = 60$ °C and $\Delta T = 18$ °C. Note that the temperature of Cell 1 is 51 °C, which is the lowest of all cells, and Cell 10 has the highest temperature of 69 °C. The voltage of Cell 10 drops almost vertically at the discharge capacity of 1.265 Ah while the other cells still maintain a relatively high voltage. This indicates that lithium-ion depletion at the negative electrode of Cell 10 occurs prior to the other nine cells. The reason behind this is that the lithium-ion concentration degradation rate increases as temperature rises, so Cell 10 with the highest temperature value will result in the lowest capacity. Moreover, since the ten cells are connected in the same series, the overall capacity is limited by the cell which has the poorest condition. In our case, the discharge process of the other cells are forced to terminate once Cell 10 has reached its end of discharge, causing the capacity of the pack to fall below expectation due to the temperature difference effect.

Here we would like to add a note about the purpose of the large temperature difference design. The temperature difference among cells could be influenced by several factors, such as the layout and design of a pack, ventilation, and boundary condition of this pack. Although we understand that it is hard to find such large temperature difference among cells when the pack is cycled at a low C-rate [42], our intention is not to illustrate a real situation. Rather, we aim to highlight the difference effect on the performance of a pack so as to stress the importance of temperature difference in future designs.

6. Experimental evidence of temperature difference effect

Besides the simulation, an experiment is also conducted to demonstrate the influence of temperature difference on the cycle life performance of series connected LIBs. In the above simulation, we connected ten cells in series each with a distinct temperature value and charged/discharged the pack for 2000 cycles. As for the experiment, we consider only a series with two cells instead of ten since it is impractical and money-consuming to investigate a 10-cell series which would require ten ovens in the lab to provide the desired temperature setup in the simulation. Details of the setup are presented in the following.

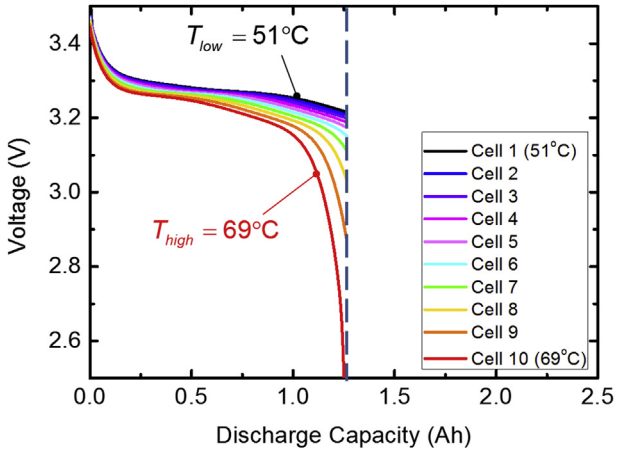

Fig. 9. The discharge curve of the ten individual cells at the 2000th cycle when $T_{avg} = 60$ °C and $\Delta T = 18$ °C.

6.1. Experimental setup

We connect two 18650 LFP 1.1 Ah cells in series and place them in different environments to create the scenario of temperature difference. One of the cells (Cell A) is exposed to the ambient, where the room temperature is kept constant at 25 °C. The other cell (Cell B) is placed inside a sealed oven with its temperature set as 55 °C. The positive side of Cell A is connected to the negative side of Cell B by an electric wire that passes through the oven's door. The other ends of the two cells are connected to the battery test station, which continuously charges and discharges the battery according to our parameter settings. The schematic diagram of the experimental setup is shown in Fig. 10.

To compare our experimental result with the one provided by the manufacturer, the charge and discharge rates of our test are given as 5 C and 10 C, respectively. Although exerting such a large amount of current on the battery makes the cell temperature depart greatly from the ambient or initial value, keeping the cells at a constant temperature is not of first importance in this experiment. Our intention is to have the two cells subject to two different temperatures/environments such that they perform dissimilarly, hoping that the influence of battery imbalance could be experimentally demonstrated.

6.2. Experimental result

Fig. 11 shows a compared result of cycle life performance. The red solid line represents the manufacturer's data, where a battery is charged and discharged by 5 C and 10 C, respectively, at an ambient temperature of 25 °C. Since, ideally, series connection does not change the total output capacity, we treat these manufacturer's data for a single cell as the performance of two cells with no temperature difference. As can be seen in the figure, the capacity fade of the cell is quite gradual. It descends at an average rate of about 0.1195 mAh cycle^{-1}, and reduces to 0.84 Ah (76% of initial capacity) after 2000 cycles.

On the other hand, our experimental result of two LIBs connected in series but with different temperatures, indicated by the blue solid line in Fig. 11, presents a more rapid decline. Due to the existence of unbalanced temperature, the capacity is fading at a faster average rate of about 0.7308 mAh cycle^{-1}, a slope that is over six times steeper when compared to the one with no temperature difference. Therefore, the capacity has dropped to a value of 0.25 Ah (24% of initial capacity) after cycled only 996 times.

At this point, it is necessary to note about the sudden drop of capacity in the experiment. As indicated by the black arrow in Fig. 11, there is a sharp decrease of capacity at the cycle number of 43 in our experiment. This is caused by a change of experimental

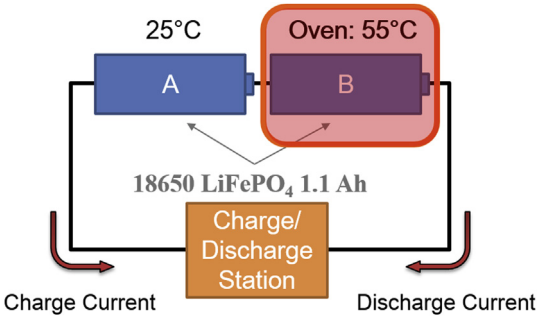

Fig. 10. The schematic diagram of the experimental setup.

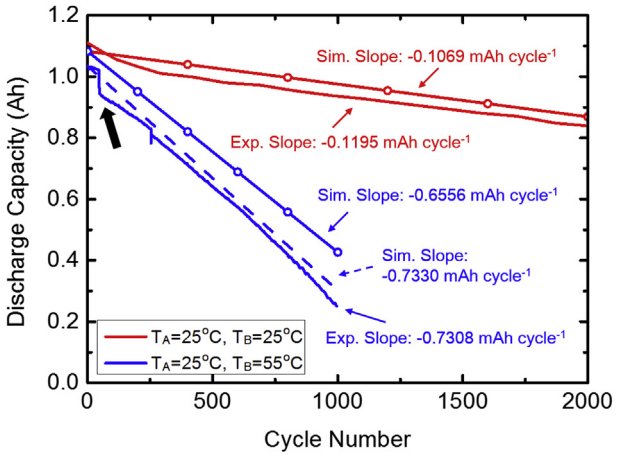

Fig. 11. The compared cycle life performance of two LIBs connected in series for (i) $T_A = T_B = 25$ °C and (ii) $T_A = 25$ °C and $T_B = 55$ °C. The solid lines are from experiment, the lines with circles are from simulation, and the dashed line represents the simulation result for the case of 25 °C/55 °C when the initial Li-ion concentration is reduced.

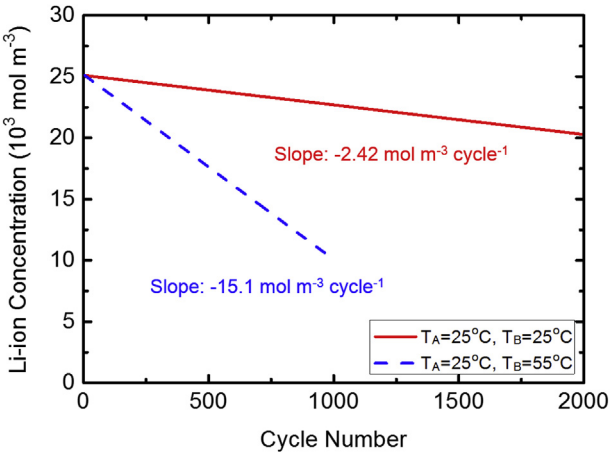

Fig. 12. Simulation of the degradation of Li-ion concentration for the 25 °C/25 °C and 25 °C/55 °C connections.

parameters that we are compelled to make after the 43rd cycle. Initially, we set a charging cut-off voltage of 7.2 V of the two series connected cells. This value is chosen by doubling the typical charging cut-off voltage of a single LFP cell, which is 3.6 V. However, due to the lithium consuming reaction as shown in Equation (9) when the LIBs are cycled, the amount of active lithium-ions which are able to intercalate into the negative electrode will be reduced. Consequently, the series connected batteries will eventually lose their ability to achieve the charging voltage of 7.2 V. Nonetheless, since we have set the cut-off voltage of 7.2 V, the charging station will still continue to force current into the batteries until the voltage is reached. As a result, the LIBs are overcharged and the cycling is terminated due to safety reasons. This will not be immediately seen after cycling the cells, because the battery with the better performance can compensate for the other cells' shortage of voltage in the first few cycles. In our case, this critical cycle is the 43rd cycle, as indicated by the black arrow. In order to continue the charging–discharging process, we have to lower the charging cut-off voltage to a smaller value of 6.7 V. This gives rise to a vertical drop of capacity at the specific cycle.

6.3. Comparison with simulation

Based on the experimental evidence that the temperature difference leads to a faster fading of a pack, we also perform an additional simulation with 18650 $LiFePO_4$ cells, which are compatible with those used in our experiment. Our simulation, illustrated in Fig. 12, demonstrates that the temperature difference generates a higher decrease in the active Li-ion concentration as time evolves. The higher decrease corresponds to a faster capacity fade during cycling, which can be observed in our simulation result, indicated by the red and blue circle points in Fig. 11.

Finally, we remark that the decrease in the charging cut-off voltage from 7.2 V to 6.7 V, reflecting a steep decrease in the discharge capacity, causes insufficient charging of the cells in the subsequent cyclings. Since we have neglected the charging process in the simulation, the charging cut-off voltage was not considered. However, we have performed another simulation by reducing the initial Li-ion concentration $C^0_{s,n,\mathrm{surf}}$ from 25,096 mol m^{-3} (in Table 1) to 24,000 mol m^{-3}, which has the same effect as that of a charging cut-off voltage decrease. The dashed line in Fig. 11, obtained from this simulation, indicates that the reduction of concentration will not only shift down the evolution curve of capacity, but it will also slightly increase the magnitude of the curve slope. From the above comparison, we conclude that a higher slope magnitude obtained from the 25 °C/55 °C experiment mainly comes from the temperature difference of the two cells, and it is partially contributed by the insufficient charging of the cells. Further experiments may be conducted to support this conclusion, and we shall consider it as our future work for a more detailed study.

7. Conclusion

We have developed a simple cycle life model that is able to simulate and quantify the capacity fade of ten series connected LIBs cycled at different temperatures. It is shown that by setting each battery with a different temperature, the whole pack's capacity is limited by the highest temperature cell. In addition, our experiment has also proved the negative impact of temperature difference on pack performance, and we have discovered that this difference also induces safety issues, i.e. overcharging of battery pack, which is extremely dangerous for LIBs [43–45].

Since our capacity fade simulation model can allow the battery temperature to be a time dependent variable, the capacity degradation of a specifically designed real-life battery pack could be predicted by constructing the corresponding three-dimensional geometry and thermal management protocol. Although such manipulation may require a large amount of computational effort, it is believed that the simulation of an actual battery pack's cycle life performance would be beneficial in optimizing the design.

Acknowledgments

This work was supported by the R.O.C. National Science Council under Grant NSC-102-2221-E-002-221.

References

[1] J. Tollefson, Nature 456 (2008) 436.
[2] K. Kang, Y.S. Meng, J. Bréger, C.P. Grey, G. Ceder, Science 311 (2006) 977.
[3] A. Chu, P. Braatz, J. Power Sources 112 (2002) 236.
[4] K. Smith, C.Y. Wang, J. Power Sources 160 (2006) 662.
[5] S. Al-Hallaj, J.R. Selman, J. Power Sources 110 (2002) 341.

[6] R. Sabbah, R. Kizilel, J.R. Selman, S. Al-Hallaj, J. Power Sources 182 (2008) 630.
[7] P. Ramadass, B. Haran, P.M. Gomadam, R. White, B.N. Popov, J. Electrochem. Soc. 151 (2004) A196.
[8] R. Darling, J. Newman, J. Electrochem. Soc. 145 (1998) 990.
[9] H.J. Ploehn, P. Ramadass, R.E. White, J. Electrochem. Soc. 151 (2004) A456.
[10] A.J. Smith, J.C. Burns, X. Zhao, D. Xiong, J.R. Dahn, J. Electrochem. Soc. 158 (2011) A447.
[11] G. Ning, R.E. White, B.N. Popov, Electrochim. Acta 51 (2006) 2012.
[12] M.B. Pinson, M.Z. Bazant, J. Electrochem. Soc. 160 (2013) A243.
[13] J. Wang, P. Liu, J. Hicks-Garner, E. Sherman, S. Soukiazian, M. Verbrugge, H. Tataria, J. Musser, P. Finamore, J. Power Sources 196 (2011) 3942.
[14] Y. Ye, Y. Shi, A.A.O. Tay, J. Power Sources 217 (2012) 509.
[15] X. Lin, J. Park, L. Liu, Y. Lee, A.M. Sastry, W. Lu, J. Electrochem. Soc. 160 (2013) A1701.
[16] R. Gogoana, M.B. Pinson, M.Z. Bazant, S.E. Sarma, J. Power Sources 252 (2014) 8.
[17] G. Singh, G. Ceder, M.Z. Bazant, Electrochim. Acta 53 (2008) 7599.
[18] D. Burch, G. Singh, G. Ceder, M.Z. Bazant, Solid State Phenom. 139 (2008) 95.
[19] P. Bai, D.A. Cogswell, M.Z. Bazant, Nano Lett. 11 (2011) 4890.
[20] N. Ravet, Y. Chouinard, J.F. Magnan, S. Besner, M. Gauthier, M. Armand, J. Power Sources 97/98 (2001) 503.
[21] B. Kang, G. Ceder, Nature 458 (2009) 190.
[22] M. Safari, C. Delacourt, J. Electrochem. Soc. 158 (2011) A562.
[23] S.Y. Chung, J.T. Bloking, Y.M. Chiang, Nat. Mater. 1 (2002) 123.
[24] A.K. Padhi, K.S. Nanjundaswamy, J.B. Goodenough, J. Electrochem. Soc. 144 (1997) 1188.
[25] N. Recham, L. Dupont, M. Courty, K. Djellab, D. Larcher, M. Armand, J.M. Tarascon, Chem. Mater. 21 (2009) 1096.
[26] J. Newman, W. Tiedemann, AIChE J. 21 (1975) 25.
[27] J. Newman, K.E. Alyea (Eds.), Electrochemical Systems, third ed., Wiley-Interscience, 2004.
[28] T.F. Fuller, M. Doyle, J. Newman, J. Electrochem. Soc. 141 (1994) 1.
[29] M. Doyle, J. Newman, A.S. Gozdz, C.N. Schmutz, J.M. Tarascon, J. Electrochem. Soc. 143 (1996) 1890.
[30] P. Arora, M. Doyle, A.S. Gozdz, R.E. White, J. Newman, J. Power Sources 88 (2000) 219.
[31] G. Ning, B.N. Popov, J. Electrochem. Soc. 151 (2004) A1584.
[32] L.O. Valøen, J.N. Reimers, J. Electrochem. Soc. 152 (2005) A882.
[33] Y.J. Liu, X.H. Li, H.J. Guo, Z.X. Wang, Q.Y. Hu, W.J. Peng, Y. Yang, R.F. Liang, J. Cent. South Univ. Sci. Technol. 39 (2008) 897.
[34] P. Ramadass, B. Haran, R. White, B.N. Popov, J. Power Sources 111 (2002) 210.
[35] P. Arora, R.E. White, M. Doyle, J. Electrochem. Soc. 145 (1998) 3647.
[36] R. Fong, U. Von Sacken, J.R. Dahn, J. Electrochem. Soc. 137 (1990) 2009.
[37] Y. Ein-Eli, B. Markovsky, D. Aurbach, Y. Carmeli, H. Yamin, S. Luski, Electrochim. Acta 39 (1994) 2559.
[38] J.R. Dahn, E.W. Fuller, M. Obravae, U. Von Sacken, Solid State Ionics 69 (1994) 265.
[39] M.C. Smart, B.V. Ratnakumar, S. Surampudi, Y. Wang, X. Zhang, B. Fultz, J. Electrochem. Soc. 146 (1999) 3963.
[40] R.J. Gummow, A. de Kock, M.M. Thackeray, Solid State Ionics 69 (1994) 59.
[41] J.M. Tarascon, W.R. McKinnon, F. Coowar, T.N. Bowmer, G. Amatucci, D. Guyomard, J. Electrochem. Soc. 141 (1994) 1421.
[42] C. Zhu, X. Li, L. Song, L. Xiang, J. Power Sources 223 (2013) 155.
[43] L. Xiao, X. Ai, Y. Cao, H. Yang, Electrochimica Acta 49 (2004) 4189.
[44] K. Kumai, H. Miyashiro, Y. Kobayashi, K. Takei, R. Ishikawa, J. Power Sources 81–82 (1999) 715.
[45] Ph Biensan, B. Simon, J.P. Peres, A. de Guibert, M. Broussely, J.M. Bodet, F. Perton, J. Power Sources 81–82 (1999) 906.

Nomenclature

a: specific interfacial area, $m^2\ m^{-3}$
A_d: reference concentration degradation rate, $mol\ m^{-3}\ s^{-1}$
A_{cell}: total effective interfacial area of cell, m^2
c: concentration of salt in electrolyte, $mol\ m^{-3}$
C_s: concentration of lithium in electrode, $mol\ m^{-3}$
C_{irr}: lithium-ion concentration loss, $mol\ m^{-3}$
D_e: electrolyte phase lithium-ion diffusivity, $m^2\ s^{-1}$
D_s: solid phase lithium diffusivity, $m^2\ s^{-1}$
E_a: activation energy, $J\ mol^{-1}$
F: Faraday's constant, 96,487 $C\ mol^{-1}$
I_{app}: applied current density, $A\ m^{-2}$
j: pore wall flux of lithium-ion, $mol\ m^{-2}\ s^{-1}$
k: reaction rate constant, $m^{2.5}\ mol^{-0.5}\ s^{-1}$
L: length, m
N: cycle number
R: gas constant, 8.314 $J\ K^{-1}\ mol^{-1}$
R_f: film resistance of SEI layer, $\Omega\ m^2$
R_s: radius of electrode particle, m
t^+: transference number
T: temperature in Kelvin, K
U^e: open-circuit potential, V
$\overline{x}$: state of charge of negative electrode
$\overline{y}$: state of charge of positive electrode
ε_f: filler volume fraction
ε_s: porous electrode volume fraction
ε_l: electrolyte volume fraction
φ_l: electrical potential of electrolyte phase, V
φ_s: electrical potential of solid phase, V
γ: Bruggman exponential, 1.5
η_s: surface overpotential, V
κ: electrolyte phase ionic conductivity, $S\ m^{-1}$
υ_+: stoichiometric coefficient of lithium-ion
σ: solid phase electric conductivity, $S\ m^{-1}$
τ: total discharge time, s

Subscript

0: value at reference temperature 25 °C
i: for component or species *i*
max: maximum
surf: surface
cc: current collector

Superscript

0: initial
eff: effective